Catalysis Today 418 (2023) 114041

Contents lists available at ScienceDirect

Catalysis Today

journal homepage: www.elsevier.com/locate/cattod

Vanadium doped Ni/Al_2O_3: Efficient and coke resistant catalysts for methane dry reforming

Marco Pizzolato [a], Giulia Da Pian [a], Elena Ghedini [a], Alessandro Di Michele [b], Federica Menegazzo [a], Giuseppe Cruciani [c], Michela Signoretto [a,*]

[a] CATMAT Lab, Department of Molecular Sciences and Nanosystems, Ca' Foscari University of Venice, and INSTM RU of Venice Via Torino, 30172 Venice, Italy
[b] Department of Physics and Geology, University of Perugia, Via Alessandro Pascoli, 06123 Perugia, Italy
[c] Department of Physics and Earth's Sciences, University of Ferrara, Via Giuseppe Saragat, 44123 Ferrara, Italy

ARTICLE INFO

Keywords:
Methane Dry Reforming
Nickel catalyst
Vanadium doped catalyst
Calcium doped catalyst
Coke

ABSTRACT

The effects of vanadium promotion on γ-alumina supported nickel catalysts were investigated for Methane Dry reforming (MDR). Three samples were compared: bare Ni/Al_2O_3 as reference, Ni-V/Al_2O_3, and Ni-V-Ca/Al_2O_3 to evaluate whether the introduction of these additional doping agents can further improve the activity and the stability of the catalyst. The catalysts were synthetized via incipient wetness impregnation and tested in MDR at 650 °C, first with a reagents ratio CH_4:CO_2:He= 1:1:18 and then CH_4:CO_2:He= 1:1:8. Fresh and spent catalysts were studied by different techniques, such as N_2 physisorption, TPR, XRD, DRUV–VIS, SEM-EDX, O_2 chemisorption and TPO. In diluted gases conditions, the introduction of vanadium is crucial to hinder catalyst deactivation by coke deposition. In particular, the formation of nanotubes was reduced, with an increase in hydrogen yield. When coupled with calcium, selectivity toward hydrogen/syngas production was improved. Under concentrated gases was highlighted how vanadium is fundamental for a higher activity, with an increase of 30% and 15% in CH_4 and CO_2 conversions, if compared with the non-doped catalyst.

1. Introduction

Hydrogen is an advantageous energy vector. It possesses the highest fuel energy content among the common fuels used, such as diesel, gasoline or methane, and its combustion produces only water as byproduct [1]. However, this gas shows many issues and challenges specially in its production procedure. Nowadays, hydrogen has been mostly produced employing fossil resources and energy intensive reactions, such as Steam Reforming of Methane (SRM) and Autothermal Reforming (ATR) [2]. Thus, this dependance by fossil resources limited the advantage of hydrogen utilization as zero emission fuel. A more sustainable approach for synthesizing hydrogen could be Methane Dry Reforming (MDR) by the following reaction (Eq. 1) [3]:

$$CH_4 + CO_2 \rightleftarrows 2CO + 2\ H_2\ \Delta H^0 = 257\ kJ/mol \quad (1)$$

This reaction allows to convert two powerful greenhouse gases, methane and carbon dioxide to syngas which is a mixture of hydrogen and carbon monoxide. For example, if the current total hydrogen produced from steam reforming (60 Mt per year) could come from MDR, it is estimated that nearly 0.5 Gt per year of CO_2 emissions could be avoided, reaching immediately the target set for 2030 from a decarbonization roadmap [4]. Therefore, MDR is a suitable reaction in a sustainable optic. However, despite the advantages, many disadvantages can be found for this reaction. For instance, applying this reaction at an industrial level could be impeded by its high endothermicity, because the reaction occurs at high temperature of around 700 °C. In fact, CO_2 is a more stable oxidizing agent, compared to steam and oxygen used in SRM and ATR, respectively [5]. Another challenge could be the occurrence of side reactions in this range of temperatures, such as [6]:

Reverse Water Gas Shift (RWGS) $H_2 + CO_2 \rightleftarrows CO + H_2O\ \Delta H^0 = 41\ kJ/mol$ (2)

Bouduard reaction $C + CO_2 \rightleftarrows 2\ CO\ \Delta H^0 = -171\ kJ/mol$ (3)

Methane Cracking $CH_4 \rightleftarrows C + 2\ H_2\ \Delta H^0 = 75\ kJ/mol$ (4)

Suitable catalysts for MDR can be based on noble metals, like Pd and Pt, and non-noble like Ni or Co. The utilization of noble metals as active phase ensures a higher activity and dispersion on the support if

* Corresponding author.
E-mail address: miky@unive.it (M. Signoretto).

https://doi.org/10.1016/j.cattod.2023.114041
Received 15 December 2022; Received in revised form 11 February 2023; Accepted 15 February 2023
Available online 21 February 2023

compared to non-noble ones, but the small abundance and hence the extremely high price limit their utilization. To avoid these problems, the use of low-cost non-noble metals should be considered and encouraged, even if they deactivate more easily. Among the non-noble metals Ni has attracted the most attention due to its high activity for MDR. However, it can also catalyze side reactions such as Bouduard (Eq. 2) or the Methane Cracking (Eq. 4) leading to the formation of different types of carbon. The formed coke could be in four different types [7]: amorphous that is oxidized at temperature between 300 °C and 500 °C; nanotubes that are oxidized at around 500 °C; graphitic that is oxidized between 700 °C and 800 °C; and graphene that is oxidized over 800 °C. To prevent the coke formation, different approaches can be followed such as the use of dopant elements and the presence of specific species on the catalyst, formed by the interaction between active metal and support. For example, it is reported that the introduction of nickel as an active phase on alumina leads to formation of spinel structure $NiAl_2O_4$ due to incorporation of Ni^{2+} in alumina lattice, thanks to the high calcination temperature [8].

Vanadium element was selected as a promotor because it has been efficiently used in the formulation of catalysts for different reactions, such as the valorization of glycerol [9], the CO and CO_2 methanation [10] and propane dehydrogenation [11]. However, in the literature, there is lack of reports on vanadium applied for MDR, if not for some isolated studies [12]. Hence, the potential benefits for such process are not still well documented. Studies on vanadium supported catalysts have determined that the supported vanadia phase is present as surface vanadium oxide species below monolayer coverage but also crystalline V_2O_5 particles can be formed [13]. Also, it has been reported that vanadium can improve the dispersion of nickel, enhancing the activity and preventing the sintering process [14]. Furthermore, the ability to adsorb the CO_2 can be improved, forming monodentate carbonates, that are the intermediates responsible of CO_2 activation [15], and inhibit the production of the polydentate ones. All these characteristics can be suitable for this work purposes. The vanadium percentage that gave the best performances in cited works is 1 wt% [9,10,12].

In addition, calcium was used as a promoter in this study because it was expected to inhibit carbon coke formation. In fact, alkali substances have been widely used as chemical agents for activation of biochar [16]. In an activation process, activation agents normally react with carbon and consume it. This could probably happen with carbon coke too, leading to its consumption from catalyst surface. Calcium can promote not only the coke removal, but also the activity of the catalyst. The presence of calcium can lead to the formation of ionic oxides increasing the CO_2 adsorption and consequently CH_4 conversions [17]. The affinity for CO_2 is due to the marked Lewis basicity of Ca species that are formed, which are responsible for good activity and stability of the catalysts [18]. Moreover, calcium addition could prevent sintering enhancing nickel dispersion [19], and it can balance alumina acidity [20]. For these reasons, in this work the percentage of calcium choose is the same of nickel (10 wt%). In addition, the cost of calcium is much less than other elements such as the lanthanides which normally are used to inhibit the coke formation. Therefore, utilization of calcium promoter in catalyst formulation can improve a low-cost and sustainable process. Indeed, CaO is widely used for industrial application such as cement production, so it can be recycled instead of being disposed in the environment [21].

Moreover, vanadium can interact with alkaline metals, forming vanadium-metal-oxygen (V-M-O) structures, modifying the basicity properties of alkaline oxides [22]. Therefore, by combining vanadium with CaO as a promoter a structure like V-Ca-O can be formed.

Herein, the introduction of vanadium will be investigated to further understand if it can enhance the properties of Ni/Al_2O_3 catalysts and can work in synergy with other known promoters such as calcium oxide. In particular, the attention will be focused on the activity, selectivity, and carbon coke resistance ability that such promoters can improve. This could give possible new insights on vanadium usage as a promoter for Methane Dry Reforming since it is still not well documented.

2. Materials and methods

2.1. Chemicals

$Ni(NO_3)_2{\cdot}6\ H_2O$ (Sigma-Aldrich, >99%); NH_4VO_3 (Sigma-Aldrich, >99%); $Ca(CH_3CO_2)_2{\cdot}H_2O$ (Sigma Aldrich, >99%); Commercial γ-alumina (Duralox Condea).

2.2. Catalysts preparation

The catalysts were prepared by incipient wetness impregnation method, to obtain 10 wt% of Ni, 1 wt% of V and 10 wt% of Ca on alumina support. The proper amounts of $Ni(NO_3)_2{\cdot}6\ H_2O$, NH_4VO_3, and $Ca(CH_3CO_2)_2{\cdot}H_2O$ precursors, were dissolved in water, the three solutions were mixed and added dropwise on γ-alumina support. The samples were dried in the oven for 18 h at 110 °C and finally calcined in the air, with a flow of 30 mL/min, at 650 °C with a heating ramp of 2 °C/min, for 4 h. The labels of all prepared catalysts are reported in Table 1.

2.3. Catalyst characterization

The metals amounts were determined via ICP-OES using a MP-AES 4200. For preparation of the sample, 50 mg of each catalyst was mineralized in a 5 mL solution of HNO_3/HCl with the ratio of 1/3 under reflux condition, for 5 h.

Specific surface areas and pore size distributions were evaluated by N_2 physisorption analyses, using the isotherms at − 196 °C obtained with a Tristar II Plus (Micromeritics). Samples were pretreated at 200 °C for 2 h using a vacuum degasser system. Surface areas were calculated using B.E.T. equation [23] while pore size distributions were determined by the B.J.H. method [24].

The Temperature Programmed Reduction (TPR) measurements were carried out using a lab-made system. 100 mg of catalyst was placed in a quartz reactor and heated in a reductive mixture flow (5% H_2/Ar 40 mL/min). The heating rate was 10 °C/min from 25° to 900°C. H_2 consumption was monitored by a Gow-Mac TCD detector.

X-ray diffraction (XRD) analyses were operated at 40 kV and 30 mA using a Philips PW 1829/00, equipped with a monochromator on the diffracted bean.

Diffuse Reflectance Ultraviolet-visible spectroscopy (DRUV–VIS) were carried out using a Cary Series UV–VIS Spectrophotometer (Agilent Technologies), with an integrating sphere in the range of 200–800 nm with 1 nm resolution.

SEM analyses of fresh and spent samples were performed after metallization with Chromium (8 nm) using a Field Emission Gun Scanning Electron Microscopy LEO 1525 ZEISS). The images were acquired by Inlens detector while elemental composition and chemical mapping were determined using Bruker Quantax EDS.

Oxygen chemisorption analyses were carried out using the same lab-made equipment presented for TPR. 50 mg of catalyst were placed in a quartz reactor, treated in H_2 at 600 °C for 1 h with a following He purge for 2 h at the same temperature. The system was cooled down to room temperature and kept at 25 °C with a thermostat to do the oxygen pulses.

Temperature programmed oxidation (TPO) on spent samples was carried out with the same equipment used for TPR, keeping the same heating rate. This time, 30 mg of catalyst was exposed in an oxidative mixture flow of 5% O_2/He.

Table 1
labels of prepared catalysts.

Catalyst	Label
Ni 10 wt% on γ-Al_2O_3	NA
Ni 10 wt% + V 1 wt% on γ-Al_2O_3	NVA
Ni 10 wt% + V 1 wt% + Ca 10 wt% on γ-Al_2O_3	NVCA

2.4. Catalytic test

Catalysts activity for MDR reaction was tested using a *Microactivity-Efficent MME1 (Process Integral Development Eng&Tech)* with a 316-steel gas-flow tubular reactor, which was directly connected to an *Agilent 8860 GC System*, with two columns in series (*Porapak N* and *Molecular Sieves 5 Å*). The volume of catalytic bed was 1 mL, composed of 150 mg catalyst diluted with SiC. The catalyst was pre-reduced at 600 °C for 1 h, under a pure H_2 flow of 30 mL/min. The reaction was carried out at 650 °C, with a GHSV of 12000 h^{-1} using He as diluent gas. The reagents ratio (CH_4/CO_2/He) was 1:1:18, under a total flow of 200 mL/min. Conversions and yields were calculated as follow (f = gas flow):

$$CH_4 \text{ conversion } \% = (fCH_4 \text{ in} - fCH_4 \text{ out}) / fCH_4 \text{ in} \bullet 100$$

$$CO_2 \text{ conversion } \% = (fCO_2 \text{ in} - fCO_2 \text{ out}) / fCO_2 \text{ in} \bullet 100$$

$$H_2 \text{ yield } \% = fH_2 \text{ out} / (2\ fCH_4 \text{ in}) \bullet 100$$

$$CO \text{ yield } \% = fCO \text{ out} / (fCO_2 \text{ in} + fCH_4 \text{ in}) \bullet 100$$

The error on conversions and yields data was 1%.

3. Results and discussion

3.1. Catalysts Characterizations

The ICP analyses were performed to measure the effective metal amounts loaded on the catalysts. As for V and Ca, values obtained are very similar to the nominal value for the three samples. As regard nickel, it deviates more (3%) for all catalysts. This can be due to the hygroscopic nature of the nickel nitrate salt used as precursor.(Table 2).

The N_2 physisorption isotherms and pore size distribution are shown in Fig. 1, and the textural properties of the catalysts are reported in Table 3.

As shown in Fig. 1, the three samples display a type IV isotherm, according to the IUPAC classification [25]. The profile of this isotherm confirms the mesoporous texture of the catalyst, due to the presence of alumina. The presence of mesopores is further confirmed by the pore size distribution, that is uniform between 1 nm and 10 nm, entering in the range of mesopores. The surface area of the latter sample is also lower than others (71 m^2/g) probably due to the presence of calcium species that partially occluded alumina pores.

TPR analyses were carried out to detect the different metal species on the catalyst surface and evaluate their interaction with the support (Fig. 2). Concerning NA sample, three peaks with increasing intensity can be observed. The first showed up very weak around 350–400 °C and can be ascribable to NiO species reduction to Ni^0 that weakly interacted with the support [26]. The peak at 550–600 °C can be assigned to reduction of NiO which interacted more strongly with alumina [27]. The last peak can be assigned to reduction of $NiAl_2O_4$ spinel specie [28]. The same peaks can be observed for NVA sample, even if NiO with strong interactions is translated at lower temperatures. This could be due to a different chemical environment of this specie because of the presence of vanadium [29]. The presence of these intense peaks for the last two species (NiO with stronger interactions and $NiAl_2O_3$) could be an advantage for stability of the catalyst, as species with a stronger interaction with the support could prevent sintering and coke formation [30]. Peaks attributable to vanadium should be present between 480 and 505 °C, 550–574 °C and 600–630 °C [31], but they are not detectable by TPR. This may be due to the low amount of this metal present inside the catalysts. We assume that vanadium reduction peaks might overlap with those of Ni. Instead, for Ca promoted catalyst, the result is similar to the one obtained for NVA sample. In this catalyst the introduction of Ca has modified the interaction between Ni and Al_2O_3. In particular, the peak relative to stronger interaction between Ni and Al_2O_3 was shifted to lower temperature, while the one relative to weaker interactions was translated to a higher temperature (400 °C). Therefore, the introduction of calcium seems to influence the nature of nickel-alumina interaction. In fact, when this element is added to these types of systems the interaction between Ni and Al_2O_3 can be weakened due to the competition between Ca and Ni to interact with alumina [32,33]. Vanadium peaks might overlap with the $NiAl_2O_4$ peak, which showed a very weak shoulder due to the second peak of vanadium reduction.

By means of XRD analysis (Fig. 3) and comparison with the Powder Diffraction File (PDF) database, it was possible to confirm the presence of NiO as bunsenite in all three catalysts (PDF card n. 47–1049) [34]. In all the samples a poorly crystalline alumina phase, attributed to cubic γ-Al_2O_3, (PDF card n. 79–1558) [3], was detected. Only in NVCA this was accompanied by abundant calcite formed by exposure to air of the catalyst. It can be reasonably assumed that vanadium could be contained in γ-alumina phase.

From the reflectance analysis of the samples (Fig. 4), the structure observed by XRD analyses can be further confirmed. For all the three samples, an intense band at 280–300 nm can be assignable to nickel species and to vanadium for the vanadium doped ones. In particular, it is ascribable to two charge transfer transitions: O^{2-} (2p) → Ni^{2+}(3d) and O^{2-} (2p) → V^{5+}(3d) [10]. In the visible range, instead, there are the d-d transitions of Ni^{2+} at 580 and 630 nm, due to Ni^{2+} tetrahedrally coordinated within $NiAl_2O_4$ structure [35] (Fig. 5a). This suggests that a possible substitution of Ni in the alumina lattice has occurred. The weak shoulders between 720 and 730 nm can be attributed to Ni^{2+} octahedrally coordinated in NiO bulk (Fig. 5b), as the absorbance at 380 nm and 430 nm [36,37].

SEM images in Fig. 6 exhibit some particles of different sizes and bigger agglomerates on the surface of the catalysts, supported on a homogeneous layer. The EDX elemental mapping (Fig. 6) shows that metals are homogeneously distributed on the alumina support, demonstrating a good dispersion of the active phase. For NVCA catalyst, the surface seems to be more similar to the NVA one, with greater agglomerations. EDX elemental mapping confirmed that the agglomeration could be mainly composed by calcium species, which also were homogeneously dispersed on the rest of surface. This evidence is in agreement with what were observed by N_2 physisorption and XRD analyses. In fact, for the NVCA catalyst, a lower surface area was measured, due to the presence of abundant calcium species, confirmed by the XRD analyses.

From chemisorption analyses it was possible to determine metallic areas and mean particle diameter for the three catalysts. What can be observed in Table 4, is that for NVCA catalyst there is a major metallic area and a minor mean diameter of nanoparticles. The minor size registered for NVCA catalyst can confirm the effectiveness of calcium introduction as promoter for a better nickel dispersion [19]. Another important aspect is that a lowering in mean diameter value was registered for NVA if compared to NA. This can suggest that the introduction of vanadium could help to a better nickel dispersion too.

Table 2
Nominal and effective metals loadings in the catalysts determined by ICP analysis.

Sample	Ni nominal loading (%)	Ni actual loading (%)	V nominal loading (%)	V actual loading (%)	Ca nominal loading (%)	Ca actual loading (%)
NA	10	7	-	-	-	-
NVA	10	7	1	0.8	-	-
NVCA	10	7	1	1	10	10

3.2. Activity test

As for catalytic performances (Fig. 7), all the catalysts display proper CH_4 and CO_2 conversions, with stable values that reached more than 80% for both reagents during 100 h of reaction time. The good stability

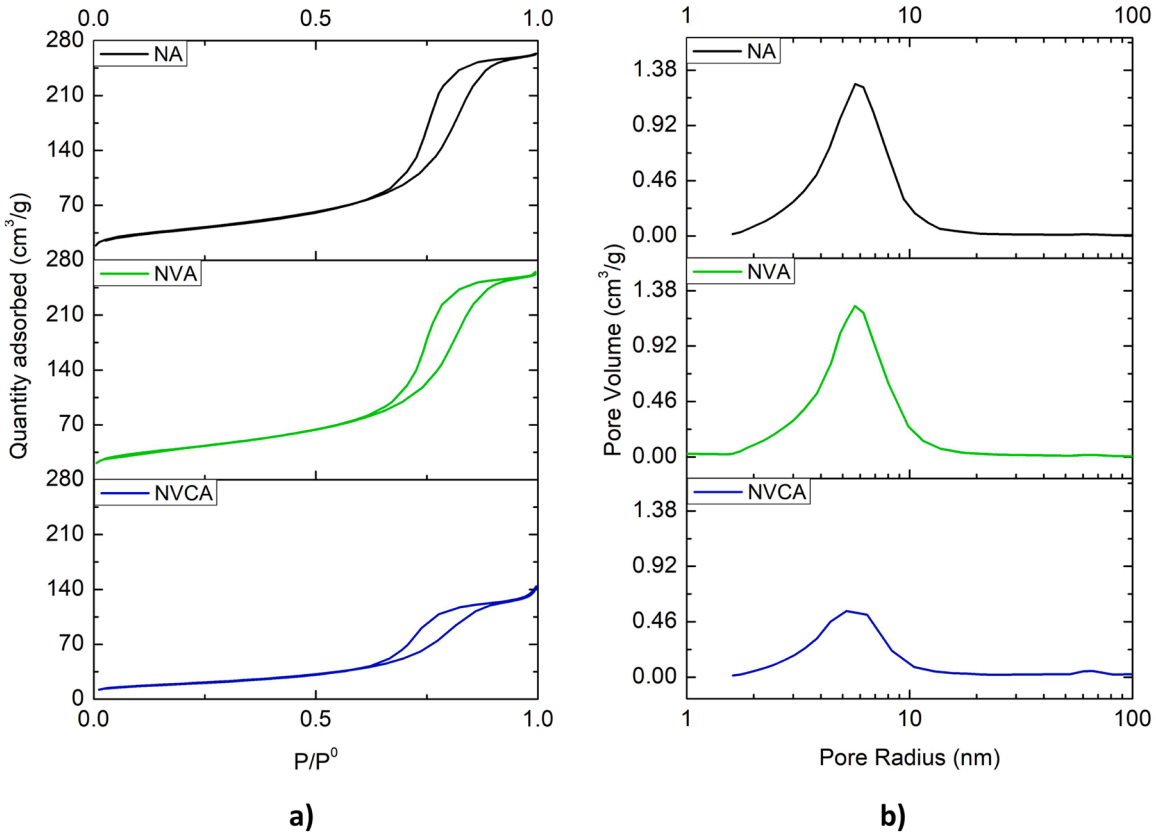

Fig. 1. a) N_2 adsorption-desorption isotherms and b) pore size distributions of NA, NVA and NVCA catalysts.

Table 3
Surface areas, pore volumes and average pore radius of the three catalysts calculated by B.E.T. and B.J.H. methods.

Sample	Surface Area (m^2/g)	Pore Volume (cm^3/g)	Average pore radius (nm)
NA	142	0.45	5
NVA	145	0.47	5
NVCA	71	0.24	5

can be ascribed to the formation of $NiAl_2O_4$ spinel structure as highlighted in DRUV-Vis spectra. This could provide more interaction between Ni and alumina hindering sintering. Despite the optimal results in terms of stability of all the samples, the best conversions were found for the promoted samples which the loss in activity is lower compared to NA. This suggests the influence of vanadium and calcium in the preservation of catalyst from deactivation through coke deposition, and a better nanoparticles dispersion as proved by chemisorption. Indeed, the result of this study was more promising compared to other two works reported on vanadium promoted catalysts for MDR [12,39]. In fact, even if it is very difficult to compare data obtained in different catalytic rigs, comparing the obtained results with the one reported by Valentini et al., is possible to observe that higher conversions were reached. These were similar to those of Lu et al. but in this study lower reaction temperatures are used. Higher yields of H_2 and CO were also obtained using promoted catalysts compared to bare NA. In fact, looking at the yields of H_2 and CO in Fig. 7(c,d) confirms that each promoter could increase the overall product yield. In particular, vanadium doping seems to be fundamental to improve hydrogen yield, because an increase of about 7% can be observed for NVA and NVCA catalysts. Lu et al. reported that vanadium can increase nickel electron cloud density, lowering the activation energy of CH_4 cracking to CH_3 and H species [39]. This value is not affected by the presence of a co-dopant. The presence of calcium species

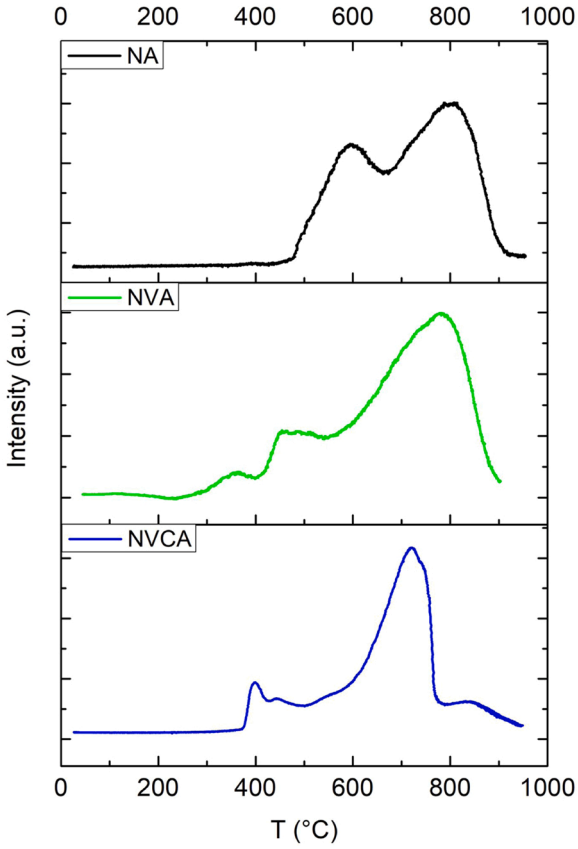

Fig. 2. TPR profiles of the catalysts.

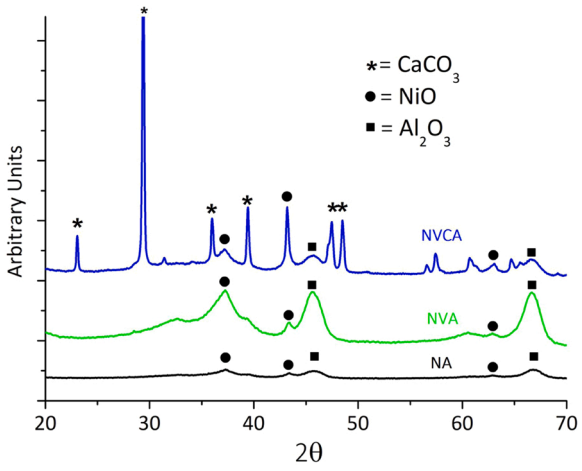

Fig. 3. XRD patterns of NA, NVA and NVCA samples.

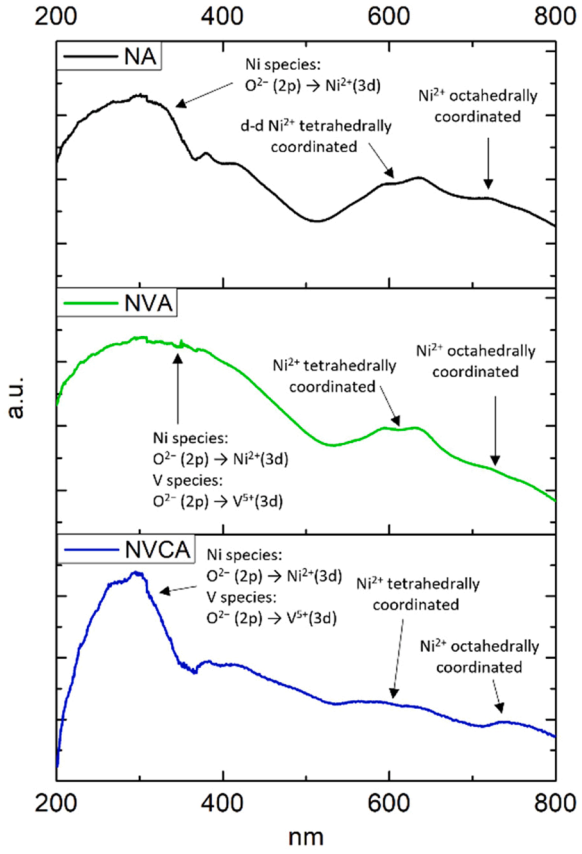

Fig. 4. DRUV–VIS spectra of the catalysts.

can also improve activity and stability of the catalyst. Calcium promotion seems to increase CO yield reaching to 62% after 100 h of reaction (yield results over 100 h for H_2 and CO are reported in Fig. S1 in the supplementary information), and as it can be seen in Fig. 7d), there is an increment in CO yield compared to NA and NVA catalysts. This increment may be ascribed to an anti-coke action of calcium. In fact, alkali elements are well known to be active in the oxidation of carbonaceous species. Thus, calcium was capable in freeing catalyst surface and increasing its stability as well.

3.3. Characterizations of spent catalysts

TPO profiles were obtained from the spent catalysts after 100 h time on stream in diluted conditions and it is shown in Fig. 8. As it can be seen, different types of carbon were probably formed on the catalytic surfaces. All the three samples display a weak peak between 300 °C and 400 °C, that can be ascribed to the presence of amorphous carbon [7]. For NA and NVA samples, a convolution of peaks in the range of 500–700 °C suggests the presence of nanotubes and graphitic coke [40]. In particular, nanotubes can be oxidized at around 500 °C, while graphitic carbon at around 700 °C. The same can be observed for NVCA, but with different behaviors. In fact, the peaks of nanotubes and graphitic carbon are well defined. However, the presence of three types of carbon on the alumina supported catalysts seems to not have affected the reactivity and stability of the catalysts. Hence, it can be stated that the best performances in keeping active phase nanoparticles free from carbon deposition were achieved by NVCA catalyst. This because it showed the best activity in diluted conditions (Fig. 7), even if at TPO carbon was detected.

From SEM images of the spent samples after 100 h time on stream in diluted conditions, a persistent presence of nanotubes can be noted on the sample surface for NA catalyst. Also, from EDX, a homogeneous distribution of the carbon can be seen, demonstrating how the catalytic surface could be poisoned by carbon deposition, during 100 h of the reaction. The obtained result can explain a lower stability of this catalyst. Fig. 9b) demonstrates that after the introduction of vanadium, some zones of the NVA catalyst surface became free from carbon nanotubes deposition, contrary to what were observed on NA sample. In addition, from EDX result, the non-homogeneous distribution of carbon was visible, demonstrating that big zones of the surface are less covered by carbon in general. The introduction of vanadium, therefore, seems to help on preventing nanotubes poisoning on nickel particles. This is an extremely important aspect since the nanotubes incapsulate Ni nanoparticles [41]. Thus, they are one of the major issues hindering the regeneration of the catalyst and the activity of the active metal phase. As concern NVCA, the presence of calcium seems to be effective because the surface of catalyst can be almost free from nanotubes, if compared with the other catalysts. EDX images report carbon distribution ascribable to nanotubes, but also to amorphous and graphitic carbon detected by TPO.

3.4. Stress tests

To better understand the behavior and the resistance of formulated catalysts, they were tested under a more concentrated flow of gas reagents. In particular, temperature and GHSV were the same to the one used for the stability tests, previously reported in Fig. 7, but the gas ratio was changed to CH_4:CO_2:He = 1:1:8.

From the trends obtained in Fig. 10, it can be seen that NVA catalyst exhibits the best performance. This catalyst was less stable than what was observed in diluted conditions, but even after 50 h of the reaction, the values of conversions were still acceptable. Even if the ratio between the reagents is 1:1, and so the same conversion is expected, the stress tests bring in evidence the role of support. The conversions depend on the affinity of reagents for the catalyst used, in this case it seems that the Ni/Al_2O_3 systems have more affinity for CO_2, converting it more than CH_4 [42]. Unlike to stability tests over 100 h, NVCA catalyst seems to be the worst under these conditions. This might be due to the high amount of calcium present in this catalyst [19] affecting the activity with more concentrated reagents. In fact, with a high amount of basic sites alongside CO_2 activation and conversion, also CH_4 decomposition is favored, leading to coke deposition [43]. Under concentrated reagents this effect could be more emphasized, leading to major carbon deposition and so less stability and activity. Also, looking at the results of stress tests, it can be concluded that the introduction of vanadium on the catalyst surface was efficient in terms of activity, if NVA and NA catalysts are compared.

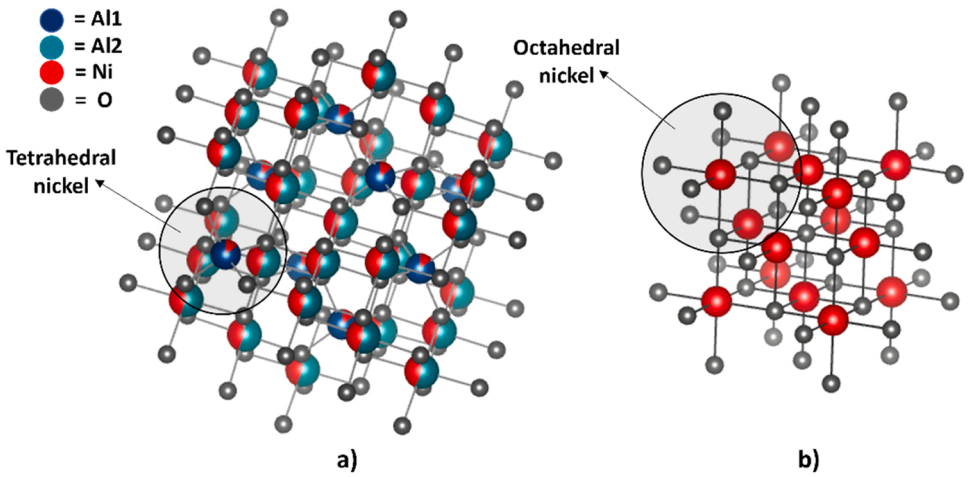

Fig. 5. a) $NiAl_2O_4$ structure; b) NiO (bunsenite) structure. Images elaborated with VESTA program [38].

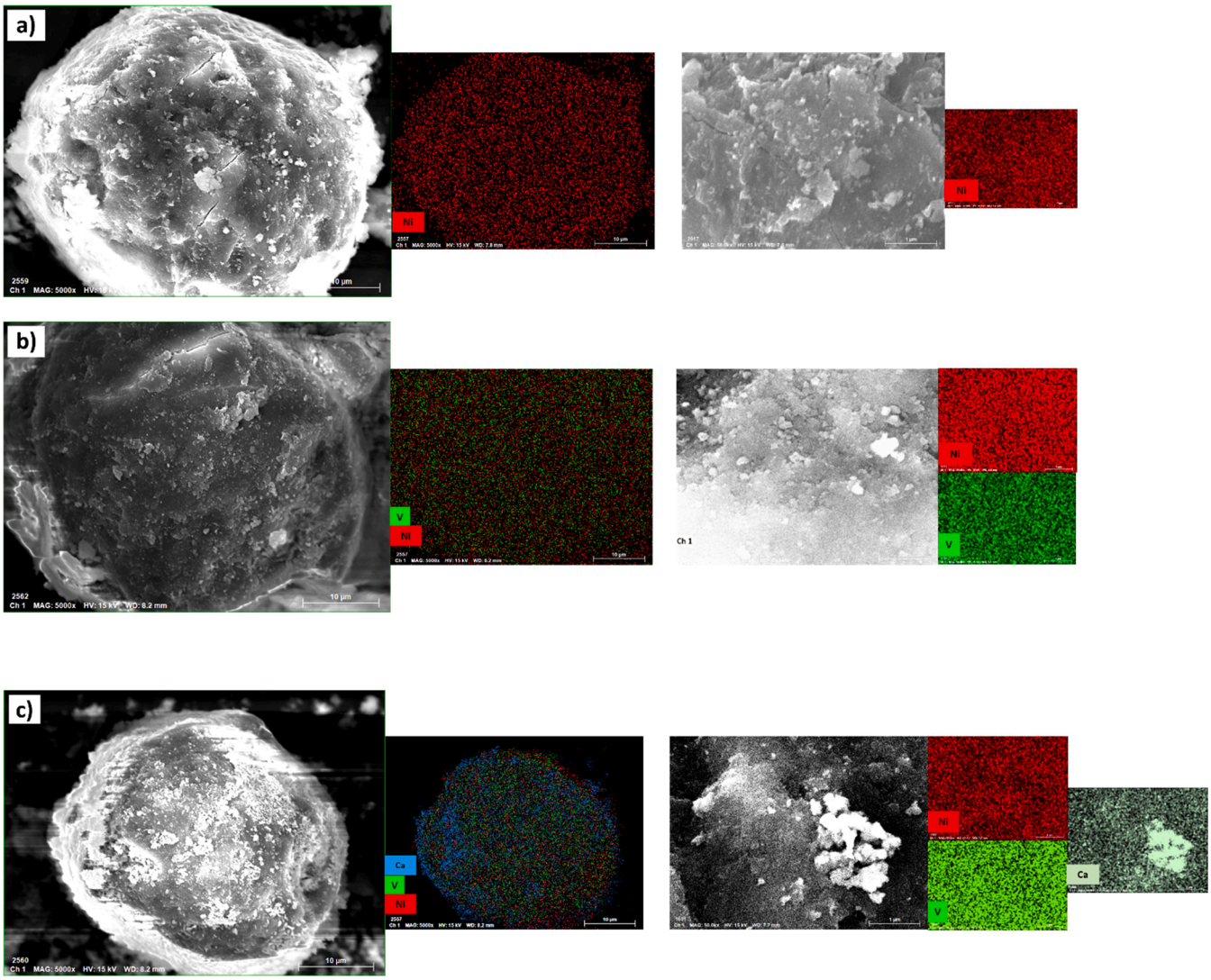

Fig. 6. EDX elemental mapping of NA (a), NVA (b) and NVCA (c).

Table 4
Values of metal area and mean diameter obtained from chemisorption.

Catalyst	Area (m^2/g of metal)	Mean diameter (nm)
NA	8	69
NVA	11	53
NVCA	47	12

Indeed, the conversion of CH_4 was increased by 30%, while CO_2 conversion was increased by 15%.

3.5. Characterizations on spent sample from stress tests

Comparing spent catalysts' TPO, (Fig. 8 and Fig. 11) it is possible to observe that the types of carbon deposits formed on catalysts are the same for all the three samples, independently by gases concentration. Only for spent NA profile could be noted some differences. In fact, under concentrated gases, there is no longer a single peak for nanotubes and graphitic coke. Between 500 °C and 600 °C a weak nanotube-associated peak is visible, as a shoulder of the more intense graphitic carbon's peak at 600–750 °C. At lower temperatures (350 °C) a slight peak is visible, ascribable to amorphous coke. NVA spent catalyst reported a very similar profile to NA one, with the same peaks and species detected by TPO on spent NVA from diluted gases test. The same can be concluded for NVCA spent catalyst. It is possible to say that the minor activity demonstrated by this catalyst during stress test is connected to presence of calcium species under concentrated gases (Par. 3.4).

From SEM-EDX (Fig. 12) it is possible to better understand the different activity behavior of the catalysts. In fact, from SEM images it could be seen that NVA catalyst's surface presents a major area free from carbon nanotubes deposition, if compared to NA and NVCA ones. In particular, NVCA is the most covered by carbon, as shown by EDX mapping, with a homogeneous coke distribution (Fig. 12 c). This can confirm that calcium enhances CH_4 decomposition leading to a major coke formation under concentrated gases (Par. 3.4). The EDX mapping on NA and NVA catalyst's grains shows a carbon distribution similar for the two samples. From this evidence, it is possible to affirm that vanadium is effective in boosting catalyst's activity. This could be due to a major ability of vanadium in preserving nickel nanoparticles free from carbon, that will deposit around them.

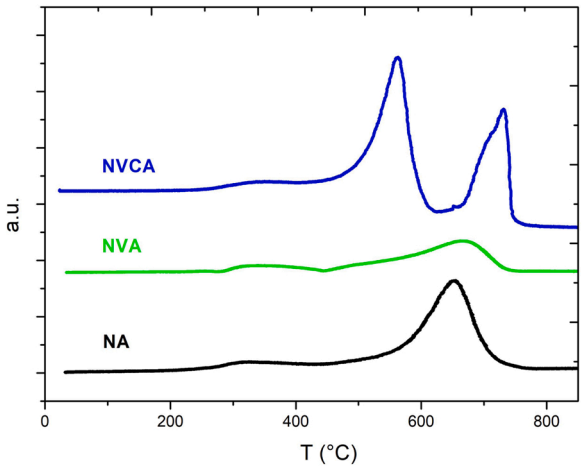

Fig. 8. TPO profiles of spent samples.

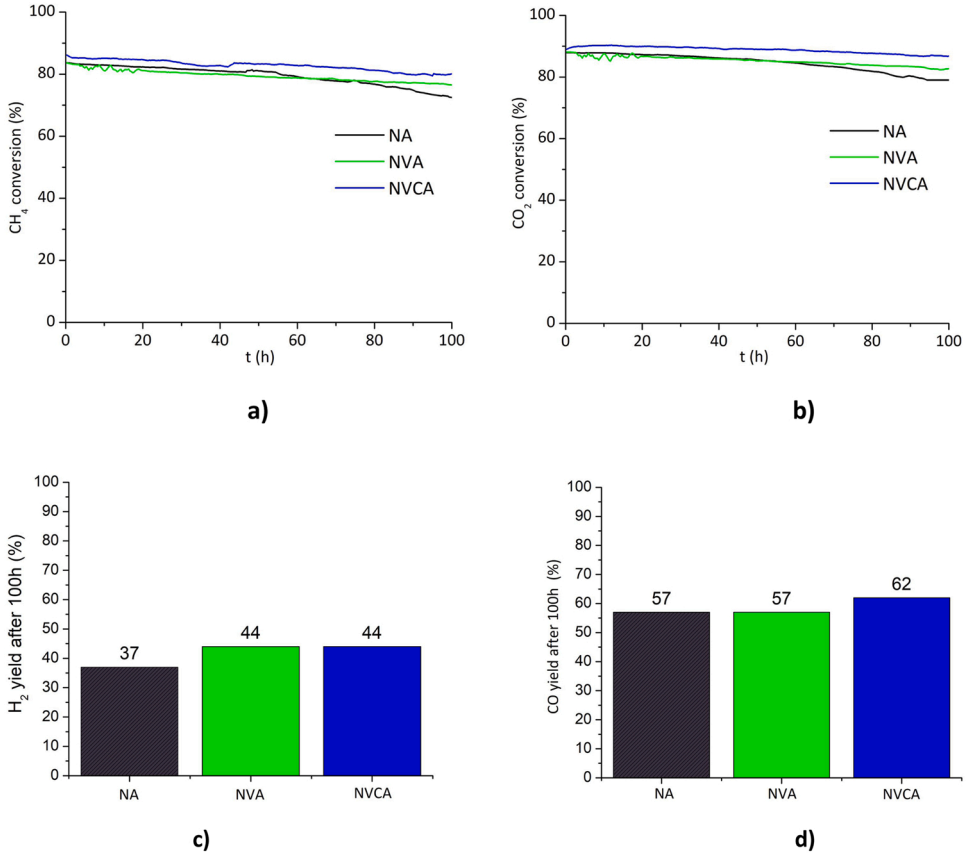

Fig. 7. Activity of the catalysts prepared, a) CH_4 conversions; b) CO_2 conversions; histograms after 100 h of reaction of c) H_2 yields and d) CO yields. Reaction conditions: 650 °C, GHSV 12000 h^{-1}, reagents ratio (CH_4:CO_2:He) 1:1:18.

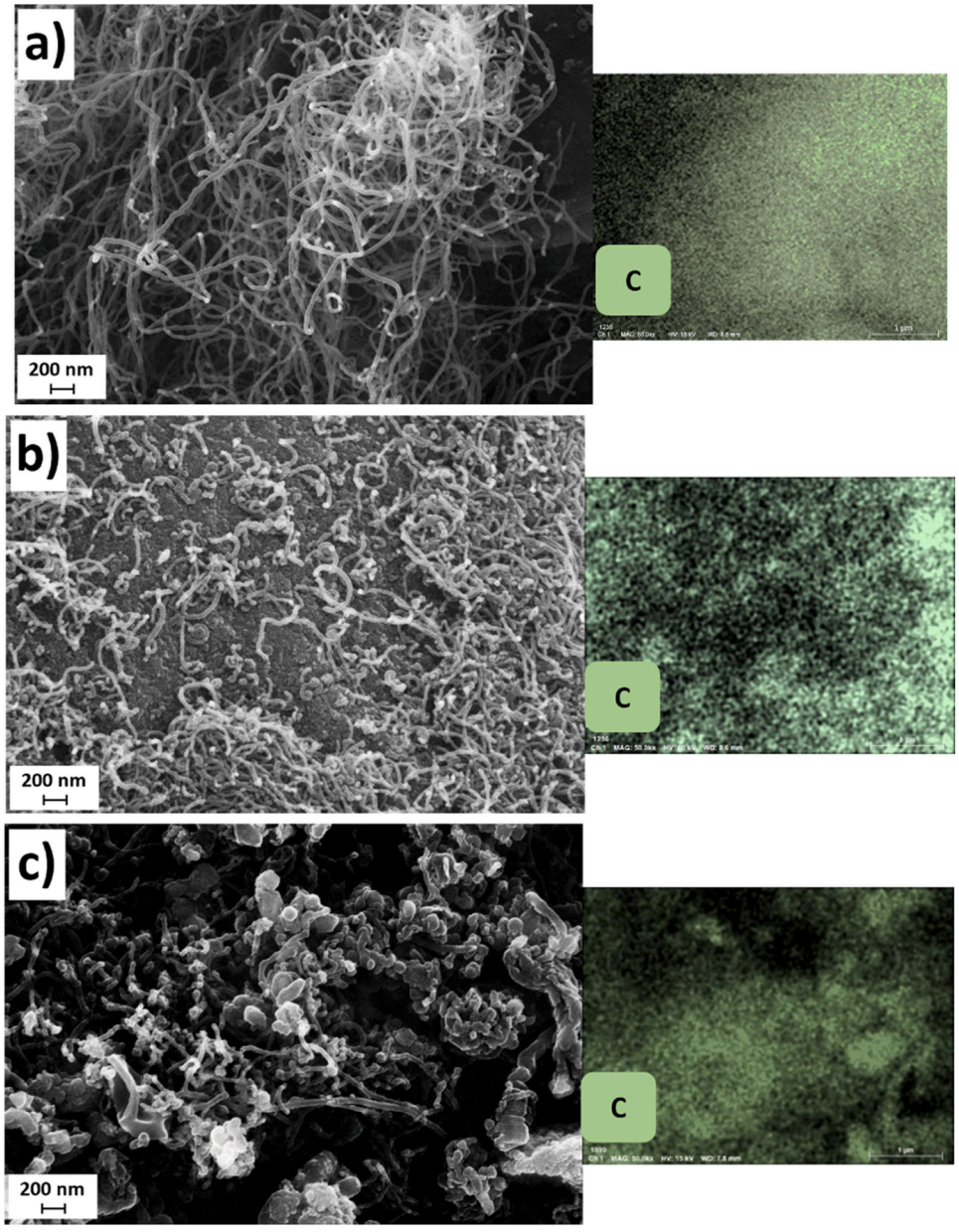

Fig. 9. SEM-EDX images of NA (a), NVA (b) NVCA (c) spent catalysts.

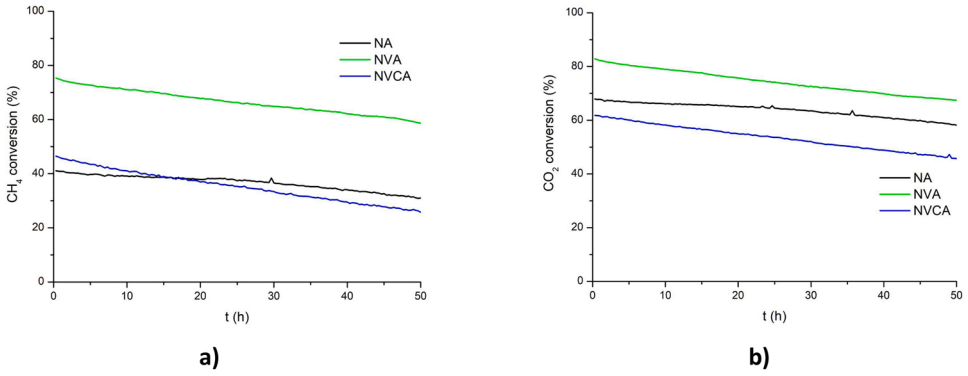

Fig. 10. Stress test results of the three catalysts, a) CH_4 conversions; b) CO_2 conversions.

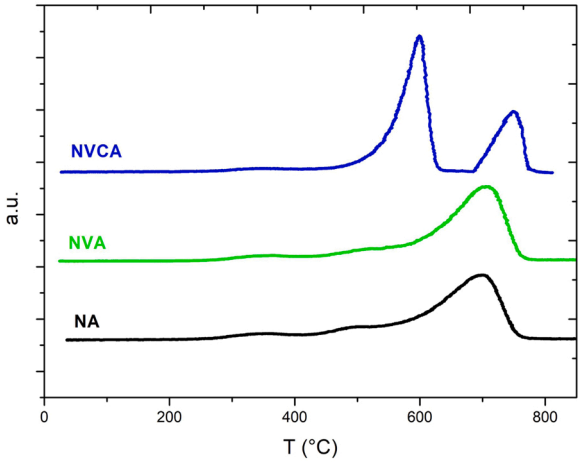

Fig. 11. TPO profiles of spent samples after stress tests.

4. Conclusions

In current study, the effects of vanadium as promoter of Ni/Al_2O_3 based catalyst for the Dry Reforming Reaction were investigated. Introduction of vanadium by incipient wetness impregnation was effective and a homogeneous metal dispersion was obtained, as confirmed by EDX analyses. Activity tests confirmed that vanadium enhanced the activity and stability of catalyst over 100 h reaction compared to the non-doped catalyst, which suffered a faster deactivation. In fact, for the promoted sample containing vanadium, also a boost of hydrogen yield was obtained in diluted conditions test. Furthermore, from spent catalysts characterizations, a lower deposition of nanotubes was detected on promoted NVA catalyst. With the introduction of Ca, this phenomenon was further enhanced as it could be seen in SEM-EDX images, but only as concern reaction in diluted gases. In fact, it was proved that gases concentration directly affects both stability and activity of this catalyst. In stress tests was further highlighted the positive effect of vanadium introduction, that led to a higher conversion of reagents with a 30% increase for CH_4, and 15% increase for CO_2. It can be concluded that vanadium is a valuable promoter for Ni/Al_2O_3 based catalysts for Methane Dry Reforming.

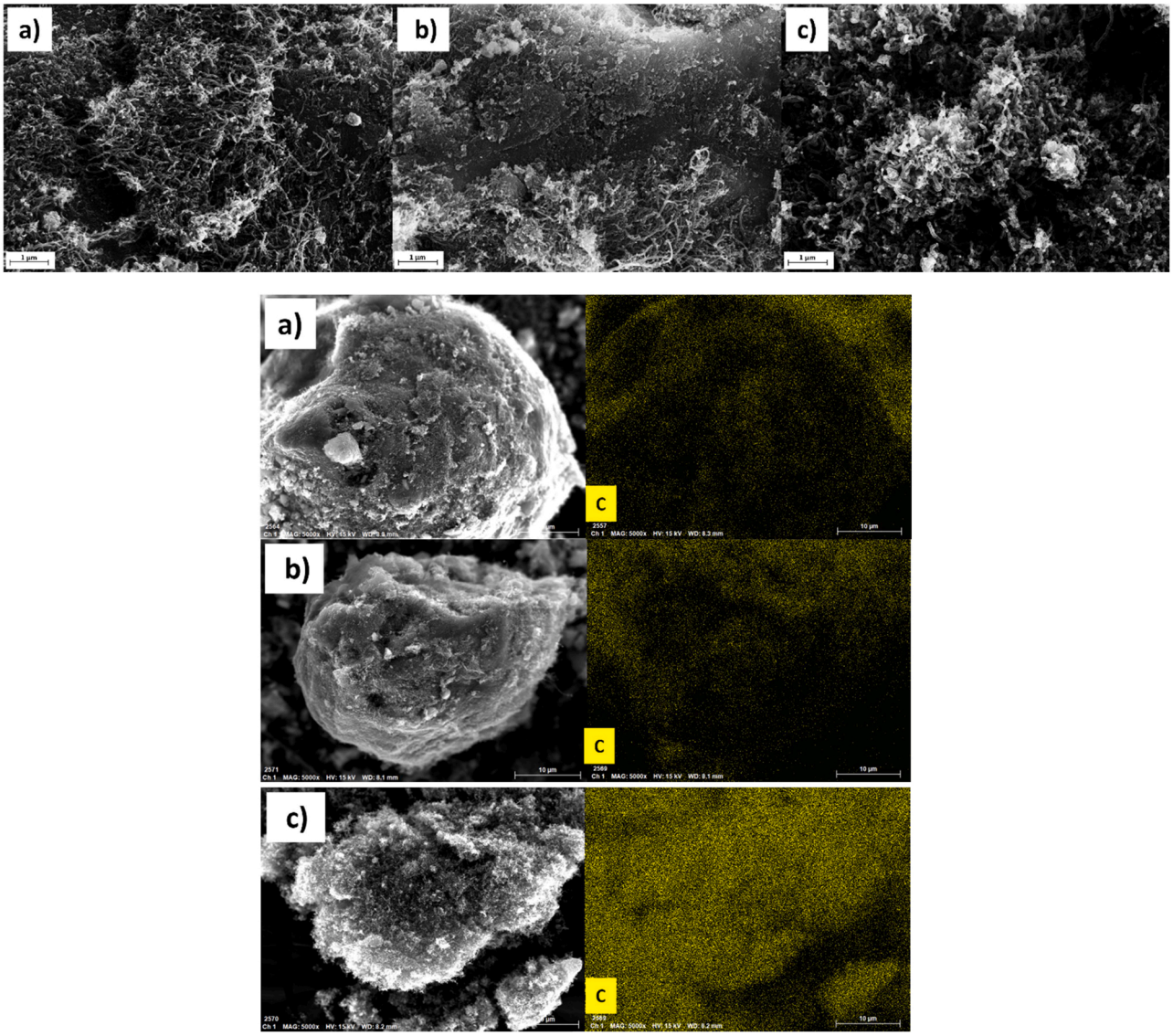

Fig. 12. SEM-EDX images of NA (a), NVA (b), NVCA (c) spent catalysts after stress tests.

CRediT authorship contribution statement

Marco Pizzolato: Conceptualization, Methodology. **Giulia daPian**: Data curation, Writing – original draft. **Elena Ghedini**: Visualization, Investigation. **Alesandro Di Michele**: Investigation. **Federica Menegazzo:** Writing – review & editing. **Giuseppe Cruciani**: Investigation, Data curation. **Michela Signoretto**: Supervision, Writing – review & editing.

Declaration of Competing Interest

The authors declare that they have no known competing financial interests or personal relationships that could have appeared to influence the work reported in this paper.

Data Availability

Data will be made available on request.

Acknowledgements

We would like to aknowledge the Doctorate in Chemistry of UniTS.

Appendix A. Supporting information

Supplementary data associated with this article can be found in the online version at doi:10.1016/j.cattod.2023.114041.

References

[1] M. Yue, H. Lambert, E. Pahon, R. Roche, S. Jemei, D. Hissel, Renew. Sustain. Energy Rev. 146 (2021), 111180.
[2] P. Nikolaidis, A. Poullikkas, Renew. Sustain. Energy Rev. 67 (2017) 597–611.
[3] N.A. Abd Ghani, A. Azapour, A.F. ad Syed Muhammad, B. Abdullah, Int. J. Hydrog. Energy 44 (2019) 20881–20888.
[4] Y. Song, E. Ozdemir, S. Ramesh, A. Adishev, S. Subramanian, A. Harale, M. Albuali, B.A. Fadhel, A. Jamal, D. Moon, S.H. Choi, C.T. Yavuz, Science 367 (2020) 777–781.
[5] N.A.K. Aramouni, J.G. Touma, B.A. Tarboush, J. Zeaiter, M.N. Ahmad, Renew. Sustain. Energy Rev. 82 (2018) 2570–2585.
[6] M. Hassan Amin, Prog. Petrochem. Sci. 2 (2018) 161–165.
[7] A.A. Lemonidou, M.A. Goula, I.A. Vasalos, Catal. Today 46 (1998) 175–183.
[8] A. Tribalis, G.D. Panagiotou, K. Bourikas, L. Sygellou, S. Kennou, S. Ladas, A. Lycourghiotis, C. Kordulis, Catalysts 6 (2016) 11–13.
[9] R.V. Lelo, G.K. Maron, A. Thesing, J.H. Alano, L. da Silva Rodrigues, B. da Silveira Noremberg, M.T. Escote, A. Valentini, L.F.D. Probst, N.L.V. Carreño, Fuel Process. Technol. 216 (2021), 106773.
[10] G. Garbarino, P. Kowalik, P. Riani, K. Antoniak-Jurak, P. Pieta, A. Lewalska-Graczyk, W. Lisowski, R. Nowakowski, G. Busca, I.S. Pieta, Ind. Eng. Chem. Res. 60 (2021) 6554–6564.
[11] P. Rybarczyk, H. Berndt, J. Radnik, M.M. Pohl, O. Buyevskaya, M. Baerns, A. Brückner, J. Catal. 202 (2001) 45–58.
[12] A. Valentini, N.L.V. Carreño, L.F.D. Probst, P.N. Lisboa-Filho, W.H. Schreiner, E. R. Leite, E. Longo, Appl. Catal. A Gen. 255 (2003) 211–220.
[13] I.E. Wachs, Dalton Trans. 42 (2013) 11762–11769.
[14] X. Lu, F. Gu, Q. Liu, J. Gao, Y. Liu, H. Li, L. Jia, G. Xu, Z. Zhong, F. Su, Fuel Process. Technol. 135 (2015) 34–46.
[15] M. Zhang, J. Zhang, Z. Zhou, S. Chen, T. Zhang, F. Song, Q. Zhang, N. Tsubaki, Y. Tan, Y. Han, Appl. Catal. B 264 (2020), 118522.
[16] X. Liu, F. Shen, R.L. Smith, X. Qi, Bioresour. Technol. 294 (2019), 122198.
[17] B. Abdullah, N.A. Abd Ghani, D.V.N. Vo, J. Clean. Prod. 162 (2017) 170–185.
[18] Y. Sun, G. Zhang, J. Liu, Y. Xu, Y. Lv, Int. J. Hydrog. Energy 45 (2020) 640–649.
[19] H. Wang, W. Mo, X. He, X. Fan, F. Ma, S. Liu, D. Tax, ACS Omega 5 (2020) 28955–28964.
[20] A. Ranjbar, M. Rezaei, J. Nat. Gas. Chem. 21 (2012) 178–183.
[21] O. el Samrout, L. Karam, K. Jabbour, P. Massiani, F. Launay, N. el Hassan, Catal. Sci. Technol. 10 (2020) 6910–6922.
[22] S. Zhang, H. Liu, Appl. Catal. A. Gen. 573 (2019) 41–48.
[23] S. Brunauer, P. Emmett, E. Teller, J. Am. Chem. Soc. (1938) 309–319.
[24] E.P. Barrett, L.G. Joyner, P.P. Halenda, J. Am. Chem. Soc. (1951) 373–380.
[25] K.S.W. Sing, Pure Appl. Chem. 57 (1985) 603–619.
[26] F. Menegazzo, M. Signoretto, F. Pinna, P. Canton, N. Pernicone, Appl. Catal. A Gen. (2012) 80–87.
[27] M. Pizzolato, G. Da Pian, E. Ghedini, A. di Michele, F. Menegazzo, G. Cruciani, M. Signoretto, Reactions 3 (2022) 634–647.
[28] Y. Ma, Y. Ma, J. Li, Q. Li, X. Hu, Z. Ye, X.Y. Wu, C.E. Buckley, D. Dong, J. Energy Inst. 93 (2020) 991–999.
[29] F. v Pinto, A. Escobar, B. De Oliveira, Y. Lam, H. Cerqueira, B. Louis, J. Tessonnier, D. Su, M. Pereira, Appl. Catal. A Gen. 388 (2010) 15–21.
[30] D.H. Song, U. Jung, Y. Kim, H. Im, T. Lee, K. Lee, K. Koo, Catalysts 12 (2022) 1–13.
[31] E.P. Reddy, R.S. Varma, J. Catal. 221 (2004) 93–101.
[32] J.A.C. Dias, J.M. Assaf, Catal. Today 85 (2003) 59–68.
[33] K.F.M. Elias, A.F. Lucrédio, E.M. Assaf, Int. J. Hydrog. Energy 38 (2013) 4407–4417.
[34] C. Pizzolitto, E. Pupulin, F. Menegazzo, E. Ghedini, A. di Michele, M. Mattarelli, G. Cruciani, M. Signoretto, Int. J. Hydrog. Energy 44 (2019) 28065–28076.
[35] S. Weber, K.L. Abel, R.T. Zimmermann, X. Huang, J. Bremer, L.K. Rihko-Struckmann, D. Batey, S. Cipiccia, J. Titus, D. Poppitz, C. Kübel, K. Sundmacher, R. Gläser, T.L. Sheppard, Catalysts 10 (2020) 1–22.
[36] G. Garbarino, S. Campodonico, A.R. Perez, M.M. Carnasciali, P. Riani, E. Finocchio, G. Busca, Appl. Catal. A Gen. 452 (2013) 163–173.
[37] R. López-Fonseca, C. Jiménez-González, B. de Rivas, J.I. Gutiérrez-Ortiz, Appl. Catal. A Gen. 437 (2012) 53–62.
[38] K. Momma, F. Izumi, J. Appl. Crystallogr. 44 (2011) 1272–1276.
[39] Y. Lu, L. Kang, D. Guo, Y. Zhao, Y. Zhao, S. Wang, X. Ma, ACS Catal. 11 (2021) 8749–8765.
[40] L.A. Schulz, L. Kahle, K. Delgrado, S. Schunk, A. Jentys, O. Deutschmann, J. Lercher, Appl. Cat. A Gen. 504 (2015) 599–607.
[41] V. Pawar, S. Appari, D.S. Monder, V.M. Janardhanan, Ind. Eng. Chem. Res. 56 (2017) 8448–8455.
[42] N. Fazila Khairudin, M. Mohammadi, A. Rahman Mohamed, Environ. Sci. Pollut. Res. 28 (2021) 29157–29176.
[43] C.O. Calgaro, O.W. Perez-Lopez, Int. J. Hydrog. Energy 44 (2019) 17750–17766.